ACS Sustainable Chemistry & Engineering

Research Article

pubs.acs.org/journal/ascecg

Light-Assisted Preparation of a ZnO/CdS Nanocomposite for Enhanced Photocatalytic H_2 Evolution: An Insight into Importance of in Situ Generated ZnS

Hui Zhao, Yuming Dong,* Pingping Jiang,* Guangli Wang, Hongyan Miao, Ruixian Wu, Linggang Kong, Jingjing Zhang, and Chi Zhang

Key Laboratory of Food Colloids and Biotechnology (Ministry of Education of China), School of Chemical and Material Engineering, Jiangnan University, 1800 Lihu Avenue, Wuxi 214122, People's Republic of China

Supporting Information

ABSTRACT: In our work, ZnO/CdS hybrid photocatalysts were prepared by a simple and reproducible photodeposition method and the content of deposited CdS can be varied by irradiation time. The ZnO/CdS photocatalysts showed good photocatalytic H_2 evolution activities in aqueous $Na_2S + Na_2SO_3$ solution. When the content of CdS loading increased to 22.91% after an irradiation time of 120 min (ZnO/CdS-T120), the highest photocatalytic activity was obtained (1725 μmol g^{-1} h^{-1}), which was about 9.2 and 34.5 times than that of single ZnO and CdS photocatalysts. At the same time, ZnO/CdS-T120 presented stable photocatalytic ability (no noticeable degradation of H_2 evolution in four repeated runs in 48 h). Compared with other reported H_2 evolution photocatalysts, ZnO/CdS-T120 showed higher H_2 evolution activity and stability. Additionally, ZnO/CdS-T120 has a good natural sunlight driven H_2 evolution ability (2077 μmol g^{-1} h^{-1}). ZnS was proved to generate on ZnO/CdS-T120 surface in process of photocatalytic H_2 evolution based on structural analyses of recycle ZnO/CdS-T120. The formation of ZnS enhanced the photocatalytic H_2 evolution activity of ZnO/CdS and extended the visible light adsorption region. Meanwhile, the generation of ZnS increased the transfer interfaces for photogenerated charge carriers and consequently promoted the separation of photogenerated electrons and holes.

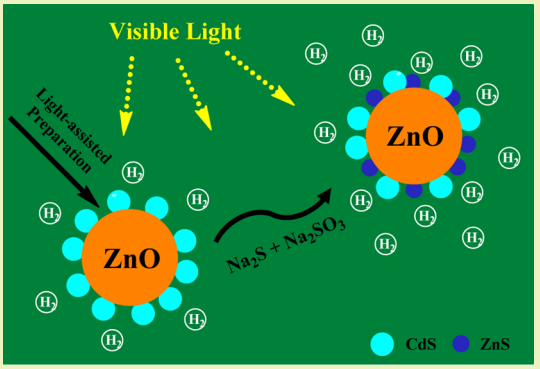

KEYWORDS: *ZnO/CdS heterostructure, Photodeposition, Photocatalyst, Water splitting, Hydrogen generation*

INTRODUCTION

With increasing awareness of the importance of energy crisis and environmental pollution, the development of green renewable energy has been greatly promoted. Hydrogen is regarded as a potential fuel to solve the fossil fuel shortage problem and environmental issues. Photocatalytic water decomposition into hydrogen is a valuable approach to utilize solar energy, which is recognized as a green and promising way to produce clean energy.[1−4] Particularly, developing visible light photocatalysts has become an attractive topic in the field of photocatalytic H_2 evolution. CdS possesses a narrow band gap (E_g = 2.4 eV) for visible light response and a suitable conduction band edge for H_2 production, which is a potential photocatalytic material for H_2 generation under visible light irradiation. Therefore, there have been some reports on CdS as a photocatalyst for visible light driven H_2 evolution.[5−10] However, CdS is subjected to serious photocorrosion process and fast recombination of charge carriers, which largely limits its scalable application. Fortunately, coupling CdS with another wide-band-gap semiconductor has been proved to be an effective strategy to suppress photocorrosion and increase charge carriers separation efficiency of CdS.[11−16] Accordingly, it is greatly desirable to introduce a proper wide-band-gap semiconductor to CdS for effective combination.

As one of the wide-band-gap semiconductors, zinc oxide (ZnO) has attracted widespread attention in photocatalytic application due to the high electron mobility, exciton binding energy (60 meV), breakdown strength, and exaction stability.[17] In this regard, incorporating CdS and ZnO into an integrated heterostructure is of great significance because the resulting products may possess improved physical and chemical properties. To date, there have been various preparation methods to obtain ZnO/CdS heterostructures with enhanced photocatalytic H_2 evolution activity, such as thermal replacement synthesis,[18,19] microwave synthesis,[20] wet chemistry synthesis,[21] cation exchange synthesis,[22] precipitation synthesis,[23] and electrospinning synthesis.[17] However, in these processes, either a postheat treatment or an additional equipment are necessary, or the complicated reaction steps are involved. In addition, we find that all these ZnO/CdS

Received: February 9, 2015
Revised: April 4, 2015
Published: April 7, 2015

DOI: 10.1021/acssuschemeng.5b00102
ACS Sustainable Chem. Eng. 2015, 3, 969−977

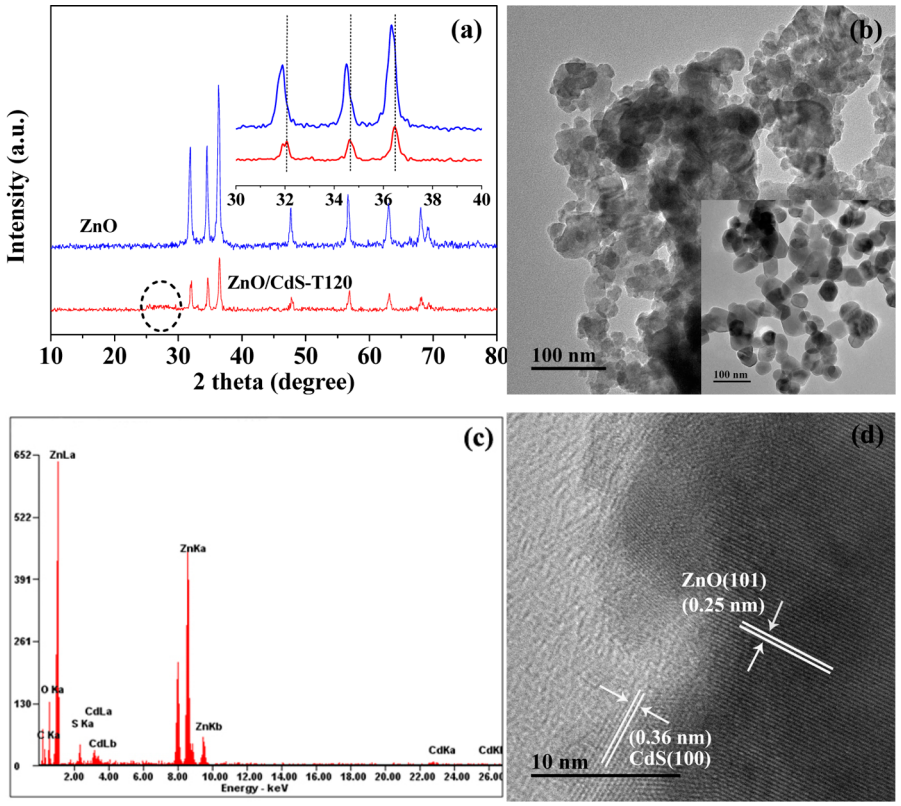

Figure 1. (a) XRD patterns of ZnO and ZnO/CdS-T120; (b) TEM image of ZnO/CdS-T120, the inset in panel b is the TEM image of ZnO; (c) EDX spectrum of ZnO/CdS-T120; (d) HRTEM image of ZnO/CdS-T120.

heterostructures were developed for enhanced photocatalytic activity from aqueous Na_2S + Na_2SO_3 solution. The surface of ZnO can undergo dissolution in alkaline sulfide solution and generate ZnS on the surface.[24] In our recent work, small sized ZnS particles were photodeposited on ZnO surfaces in the process of photocatalytic H_2 evolution using Na_2S + Na_2SO_3 as a hole scavenger, and the generative ZnS particles significantly increased the separation of photogenerated electrons and holes and were responsible for the adsorption in visible light region.[25] It may be expected that ZnS possibly forms on ZnO/CdS surface due to the presence of ZnO and participates in the photocatalysis reaction when ZnO/CdS hybrid photocatalysts are applied in H_2 evolution system with Na_2S + Na_2SO_3 hole scavenger. This point has not attained much attention to date. However, in ZnO/ZnS/CdS ternary photoelectrochemical system, the presence of ZnS promotes the separation of photogenerated electrons and holes and extends the range of the excited spectrum.[26]

Herein, in this work, ZnO/CdS nanocomposite was prepared by a simple and reproducible photodeposition method. The content of CdS can be varied by the adjustment of irradiation time. The ZnO/CdS was utilized as a photocatalyst in photocatalytic H_2 evolution from aqueous Na_2S + Na_2SO_3 solution. The photocatalytic H_2 evolution activity and stability for ZnO/CdS under visible light irradiation were investigated. At the same time, the natural sunlight driven H_2 evolution activity for ZnO/CdS was also evaluated. Furthermore, the structural analyses of recycle ZnO/CdS confirmed that ZnS particles generated on ZnO/CdS surface in photocatalytic H_2 evolution process, and the effects of generative ZnS on H_2 evolution activity and optical adsorption property were discussed in detail. The possible mechanisms were proposed for ZnO/CdS in photocatalytic H_2 generation system. The formation of ZnS on the surface increases the transfer interfaces for photogenerated charge carriers and consequently promotes the separation of photogenerated electrons and holes.

EXPERIMENTAL SECTION

Preparation. The ZnO/CdS nanoheterostructures were prepared by the following two steps: ZnO nanoparticles were first prepared according to our previous work.[25] CdS particles were subsequently deposited on ZnO through a photodeposition method. In brief, 100 mg of ZnO particles, 30 mg of S_8, and 450 mg of $Cd(NO_3)_2{\cdot}4H_2O$ were added in a mixture solution of 30 mL of ethanol and 20 mL of water. The suspension was bubbled with nitrogen for 2 h in the dark. Irradiation was carried out for given period of time (0−180 min) with a 300 W xenon lamp at room temperature. Then products were filtered, washed with water and ethanol, and dried in air. The resulting samples were denoted as ZnO/CdS-TX, where X referred to the irradiation time (min).

Characterization. To identify the composition and phase of sample, X-ray diffraction (XRD) patterns were recorded on a D8 X-ray diffractometer (Bruker AXS, German). Transmission electron microscopy (TEM) imaging was collected on a JEM-2100 transmission electron microscope (JEOL, Japan) to examine the morphology and size of sample. Energy-dispersive X-ray spectroscopy (EDX) was taken on the TEM instrument. To detect the chemical composition and electronic structure of sample, X-ray photoelectron spectroscopy (XPS) analysis was conducted using an ESCALAB 250 Xi (Thermo, USA) X-ray photoelectron spectrometer with Al Kα line as the excitation source ($h\nu$ = 1484.6 eV) and adventitious carbon (284.6 eV for binding energy) was used as reference to correct the binding energy of sample. UV−vis diffuse reffectance spectra were measured on a UV-3600 (Shimadzu, Japan) spectrophotometer. Inductively coupled plasma atomic emission spectrometer (ICP-AES, Leeman Prodigy, USA) was used to detect the element content in the sample. Elemental mapping was examined using EDX analysis on a

DOI: 10.1021/acssuschemeng.5b00102
ACS Sustainable Chem. Eng. 2015, 3, 969−977

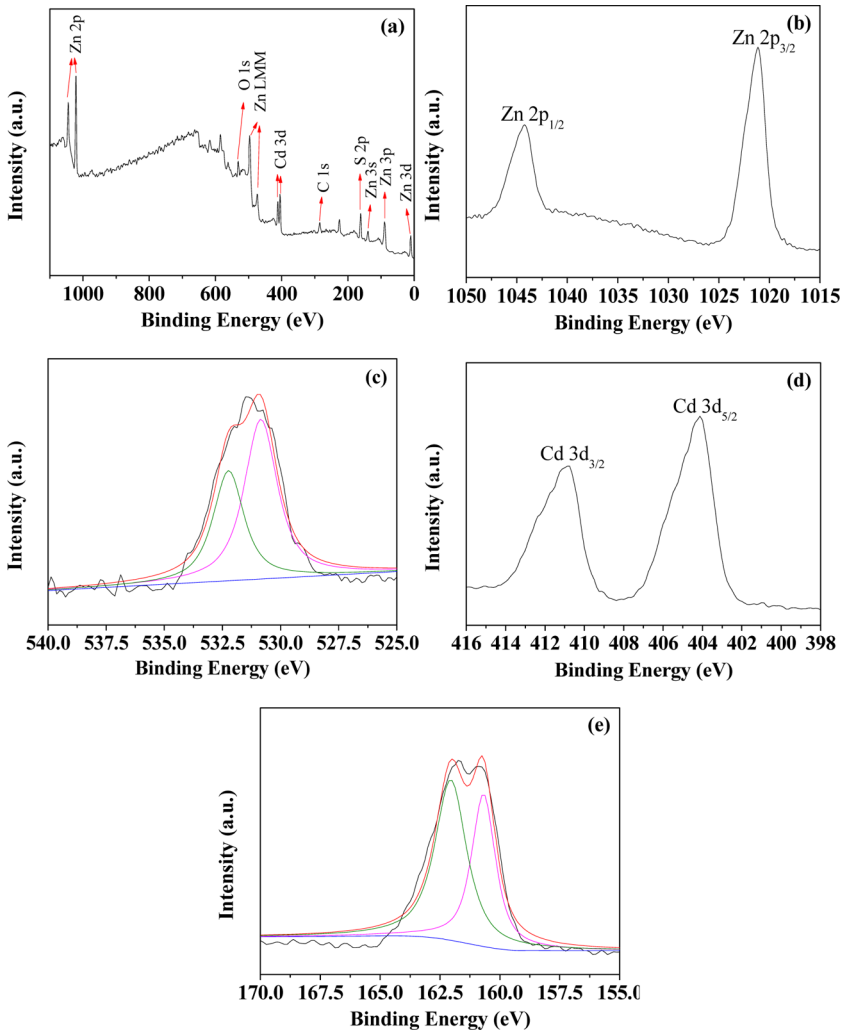

Figure 2. Survey scan XPS spectrum in the binding energy range 0−1100 eV (a) and high-resolution spectra of Zn 2p (b), O 1s (c), Cd 3p (d), and S 2p (e) for ZnO/CdS-T120.

Tecnai G2 F20 scanning transmission electron microscopy (STEM, USA) instrument.

Photocatalytic Hydrogen Production. The photocatalytic experiments were performed in a 37 mL flask at ambient temperature using a 300 W Xe lamp equipped with UV cutoff filter (λ > 400 nm). The intensity of the light source was estimated to be 0.6 W cm^{-2}. 10 mg of ZnO/CdS was added to an aqueous solution (total volume = 10 mL) containing 0.35 M Na_2S and 0.25 M Na_2SO_3. Before each experiment, the suspension was purged with a gas mixture of nitrogen and methane ($V_{nitrogen}$:$V_{methane}$ = 4:1) for 40 min to remove air. Methane served as the internal standard. Hydrogen gas evolution was measured by gas chromatography (SP-6890, nitrogen as a carrier gas) with a thermal conductivity detection (TCD) instrument.

RESULTS AND DISCUSSION

Formation and Structural Characteristics. In this work, CdS was photodeposited on the surface of ZnO by the reduction of Cd^{2+} ions to Cd^0 followed by the successive reaction with S_8.[27] In the dark, Cd^{2+} ions were adsorbed on ZnO surface for equilibrium. Under the light irradiation, ZnO was excited in which the interband transition was initiated to generate electron−hole pairs (eq 1.1). Ethanol acted as a hole scavenger. The valence band holes escaping the recombination oxidized ethanol to $\cdot C_2H_4OH$ radical (eq 1.2) that injected another electron to the conduction band of ZnO to produce CH_3CHO and H^+ (eq 1.3) due to the strong reduction power for $\cdot C_2H_4OH$ radical.[27] The electrons accumulated in the conduction band of ZnO reduced the Cd^{2+} ions adsorbed preferentially on ZnO to Cd^0 (eq 1.4). The following reaction of Cd^0 and S_8 yielded CdS (eq 1.5).

$$ZnO + h\nu \rightarrow ZnO(e_{CB}^- + h_{VB}^+) \quad (1.1)$$

$$C_2H_5OH + h_{VB}^+ \rightarrow \cdot C_2H_4OH + H^+ \quad (1.2)$$

$$\cdot C_2H_4OH \rightarrow CH_3CHO + H^+ + e_{CB}^- \quad (1.3)$$

$$Cd^{2+} + 2e_{CB}^- \rightarrow Cd^0 \quad (1.4)$$

$$8Cd^0 + S_8 \rightarrow 8CdS \quad (1.5)$$

The XRD patterns of ZnO and ZnO/CdS-T120 are given in Figure 1a. ZnO/CdS-T120 showed the characteristic diffraction peaks of hexagonal wurtzite ZnO (JCPDS No. 36-1451) at 31.8, 34.2, 36.3, 47.5, 56.5, 62.9, 66.4, 69.1, 72.6, and 77.0°, while the weak wide diffraction peaks in the range of 24−30° were indexed to aggregated (100), (002), and (101) planes of hexagonal wurtzite CdS (JCPDS No. 65-3414). Different peak related to impurity was not observed. In comparison with pure ZnO, the decreased peak intensity of ZnO in ZnO/CdS-T120

DOI: 10.1021/acssuschemeng.5b00102
ACS Sustainable Chem. Eng. 2015, 3, 969−977

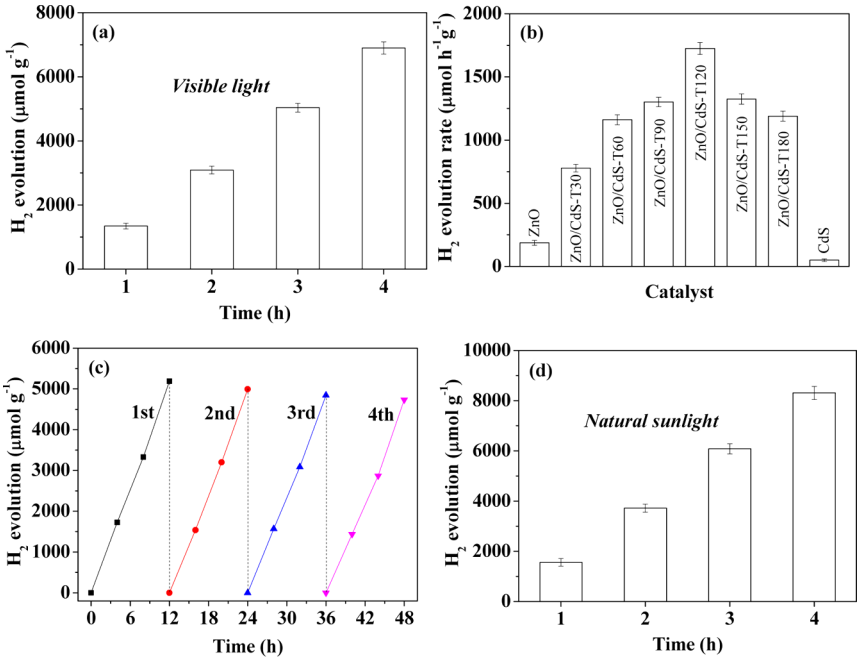

Figure 3. (a) Visible light driven photocatalytic hydrogen production by ZnO/CdS-T120; (b) visible light driven photocatalytic hydrogen production rate by ZnO, CdS, and ZnO/CdS composites with different CdS loading; (c) visible light driven photocatalytic hydrogen production by ZnO/CdS-T120 during 48 h with evacuation every 12 h (sacrificial agents were also renewed every 12 h); (d) sunlight driven photocatalytic hydrogen production during 4 h in Wuxi city on July 22, 2014, outdoor temperature, 25−32 °C; time, 10:00−14:00.

illustrated that the formation of CdS on the surface tended to lower the crystallization of ZnO. Additionally, after CdS loading, the ZnO diffraction peaks shifted to high angle due to strong phase interaction. The increase of CdS diffraction peaks and decrease of ZnO diffraction peaks were positively relative to the irradiation time (see the Supporting Information, Figure S1). As the TEM image showed in Figure 1b, CdS particles with size of 10−20 nm were deposited on ZnO surface after irradiation for 120 min. With the prolongation of irradiation time, the sizes of deposited CdS particles increased (see the Supporting Information, Figure S2). According to EDX spectrum (Figure 1c), the elements Zn, Cd, O, and S were confirmed and the atomic percents of S and O were similar to that of Cd and Zn, respectively, further indicating the ZnO/CdS composite structure. Figure 1d demonstrates a representative high-resolution TEM micrograph of ZnO/CdS-T120. The observed lattice fringes with the spacing of 0.25 and 0.36 nm were in good agreement with the interplanar spacings of the (101) and (100) planes of hexagonal wurtzite ZnO and CdS, respectively. The weight percent of CdS was determined to be 22.91% in ZnO/CdS-T120 based on the ICP-AES analysis results. The optical absorption spectra of ZnO/CdS under different irradiation times (see the Supporting Information, Figure S3) demonstrated that an increase in the irradiation time resulted in the enhanced intensities of visible adsorption band and gradual red shifts in the absorption edge.

The chemical composition and electronic structures of ZnO/CdS-T120 were analyzed typically by XPS. Figure 2a shows the scan survey spectra for the representative ZnO/CdS-T120. All of the peaks on the curve can be ascribed to Zn, O, Cd, S, and C elements. The presence of C element mainly came from the hydrocarbon contaminants that commonly existed for XPS. Therefore, it can be concluded that the sample was composed of Zn, O, Cd, and S, which was consistent with the XRD results. The positions of Zn $2p_{3/2}$ and Zn $2p_{5/2}$ peaks for ZnO/CdS-T120 (Figure 2b) were at about 1021.1 and 1044.2 eV with a spin orbit separation of 23.1 eV, which confirmed that Zn element existed mainly in the form of Zn^{2+} on the sample surface. Figure 2c shows the O 1s peak for ZnO/CdS-T120, which can be fitted into two peaks. The lower energy peak located at 530.8 eV corresponded to the oxygen atoms coordinated with Zn atoms, while the higher energy peak centered at 532.2 eV can be ascribed to the oxygen adsorbed on ZnO/CdS-T120 surface. The high-resolution XPS spectrum of the Cd orbital region (Figure 2d) presented the binding energies of Cd $3d_{5/2}$ and Cd $3d_{3/2}$ peaks at 404.1 and 410.8 eV, respectively. The splitting energy of 6.7 eV between Cd $3d_{5/2}$ and Cd $3d_{3/2}$ was a typical value for Cd^{2+} in CdS.[17] The S 2p peak was fitted into two peaks (Figure 2e). Their positions at about 160.7 and 162.1 eV were indications of S^{2-} in CdS.

Catalytic Performance. Figure 3a shows the photocatalytic activity of ZnO/CdS-T120 for H_2 generation. The H_2 production enhanced with the increase of irradiation time. During 4 h, the corresponding H_2 evolution was 6900 μmol g^{-1} without any cocatalyst. For comparison, the H_2 evolution activities for ZnO/CdS heterstructures with different CdS loadings were investigated, shown in Figure 3b. The CdS loading amount increased with irradiation time in preparation of ZnO/CdS photocatalysts (see the Supporting Information, Table S1). With the increase of CdS loading amount to 22.91 wt % (ZnO/CdS-T120), the H_2 evolution rate enhanced to 1725 μmol g^{-1} h^{-1}. However, the H_2 evolution activity for ZnO/CdS gradually decreased with the further increasing CdS loading, which was possibly due to the decreased oxidation reaction sites on the ZnO surface by postdeposited CdS. Obviously, ZnO/CdS-T120 demonstrated the highest H_2 evolution rate, which was about 9.2 and 34.5 times than that of single ZnO and CdS, respectively.

In view of practical applications, besides catalytic activity, the stability and durability are also indispensable to photocatalysts.

DOI: 10.1021/acssuschemeng.5b00102
ACS Sustainable Chem. Eng. 2015, 3, 969−977

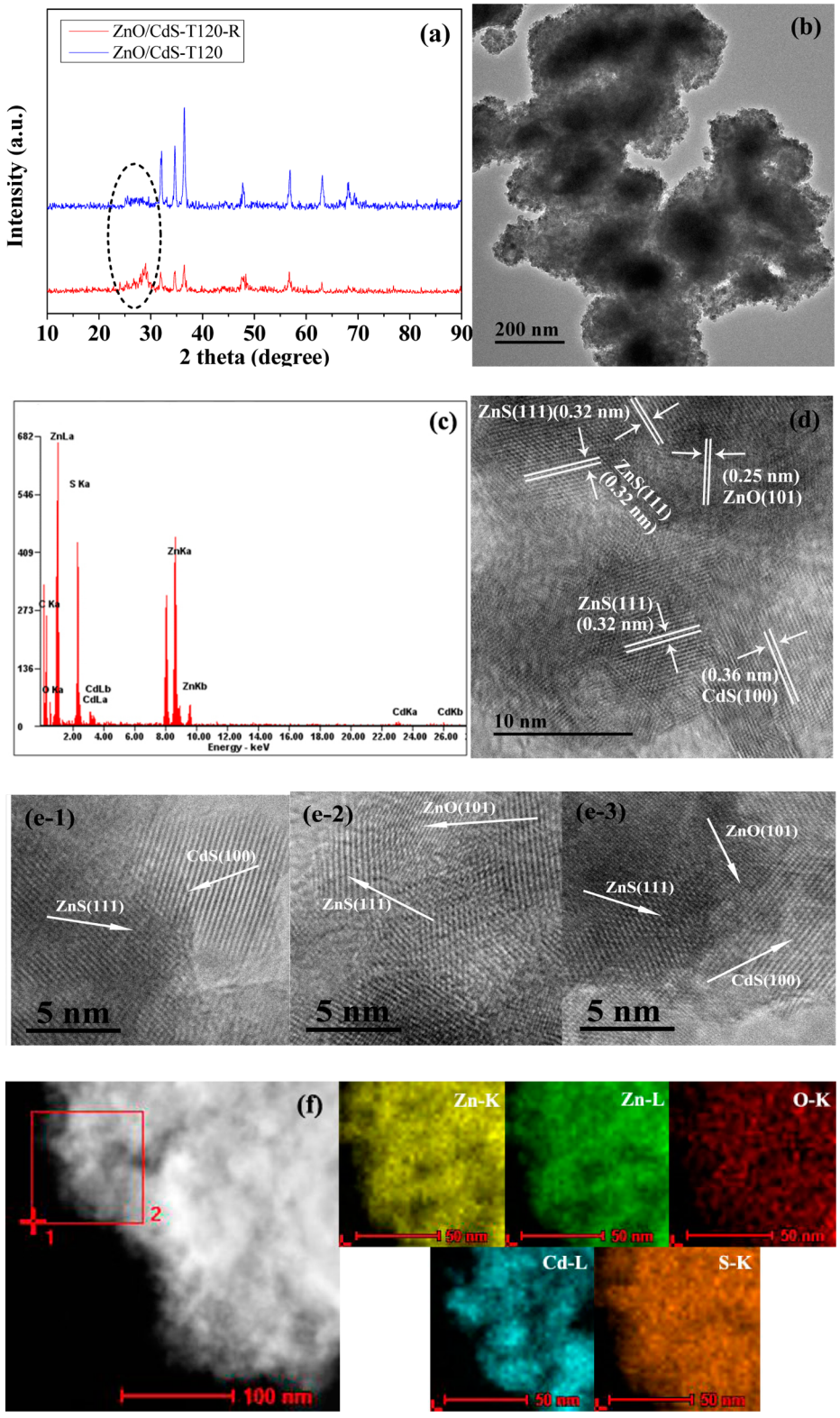

Figure 4. (a) XRD patterns of ZnO/CdS-T120 and ZnO/CdS-T120-R; (b) TEM image of ZnO/CdS-T120-R; (c) EDX spectrum of ZnO/CdS-T120-R; (d) HRTEM image of ZnO/CdS-T120-R; (e) typical HRTEM images of CdS−ZnS interfaces (e-1), ZnO−ZnS interfaces (e-2), and CdS−ZnO−ZnS interfaces (e-3); (f) STEM image and EDX elemental mapping images of Zn, O, Cd, and S of ZnO/CdS-T120-R.

To evaluate the stability and durability of ZnO/CdS-T120, we performed the time-circle H_2 evolution experiment. Figure 3c presents the H_2 evolution as the function of irradiation time. The total photocatalytic H_2 amount of ZnO/CdS after 48 h of reaction is about 19 818 μmol g^{-1}. No noticeable degradation of photocatalytic H_2 evolution was detected in four repeated runs for the whole photocatalytic reaction, indicating the good stability and durability of the ZnO/CdS-T120 sample for photocatalytic H_2 production. In addition, in comparison with other recently reported H_2 evolution photocatalysts (see the

DOI: 10.1021/acssuschemeng.5b00102
ACS Sustainable Chem. Eng. 2015, 3, 969−977

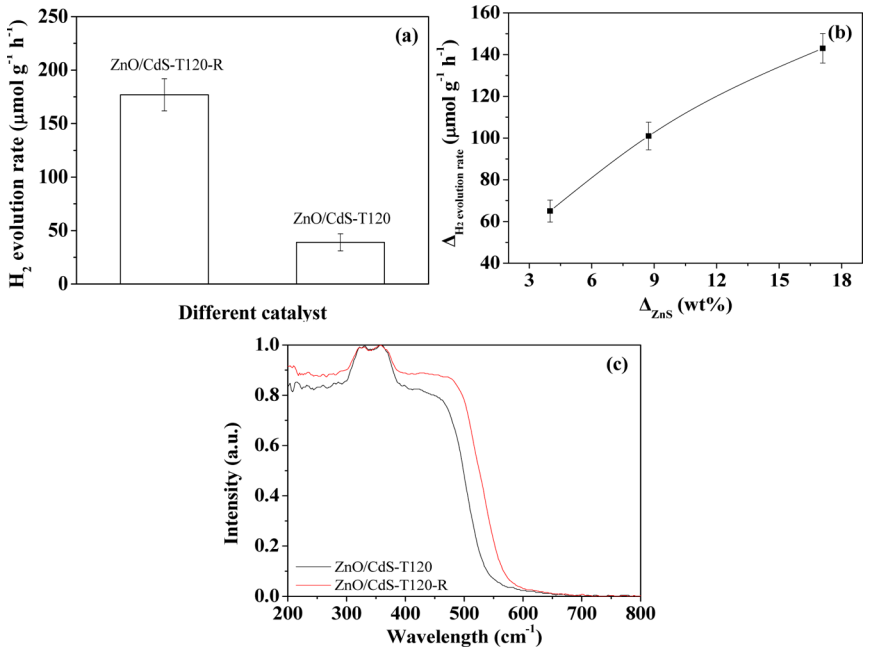

Figure 5. (a) Photocatalytic H_2 evolution rate for ZnO/CdS-T120 and ZnO/CdS-T120-R using sulfur-free triethanolamine (10 vol %) as a hole scavenger; (b) effect of generative ZnS content on H_2 evolution rate using sulfur-free triethanolamine (10 vol %) as a hole scavenger; (c) UV−vis diffuse reflectance spectra of ZnO/CdS-T120 and ZnO/CdS-T120-R.

Supporting Information, Table S2), ZnO/CdS-T120 showed higher H_2 evolution activity and stability. These results illustrated that the ZnO/CdS-T120 was among most robust photocatalysts for H_2 evolution.

The ultimate goal of photocatalyst was high-efficiency utilization of natural sunlight and solar energy. Therefore, H_2 evolution experiment was also conducted with ZnO/CdS-T120 photocatalyst under direct sunlight irradiation outdoors (see the Supporting Information, Figure S4). As shown in Figure 3d, the H_2 production significantly increased with the prolongation of sunlight irradiation time. During 4 h, H_2 evolution reached 8308 μmol g^{-1}, which was higher than that under visible light irradiation from Xe lamp. These results indicated that ZnO/CdS-T120 was a robust catalyst for sunlight-driven H_2 evolution. Such heterostructures can be promising candidates in efficient sunlight photocatalysts and potential technological applications.

Role of ZnS. The generation of ZnS took place in the photocatalytic H_2 evolution process with ZnO/CdS photocatalyst. In our previous work,[25] we had reported the in situ generation of ZnS on the surface of ZnO in the photocatalytic H_2 production process using $Na_2S + Na_2SO_3$ solution as a hole scavenger. When visible light was illuminated on the surface of ZnO/CdS, ZnO/CdS was excited with the generation of the hole−electron pairs (eq 2.1). The surface of ZnO underwent dissolution in alkaline sulfide solution for the formation of ZnS.[24] $Na_2S + Na_2SO_3$ solution acted as a hole scavenger by three possible routes (eqs 2.2, 2.3, and 2.4).[25,28] The production of S_2^{2-} ions efficiently reacted with SO_3^{2-} ions with the generation of $S_2O_3^{2-}$ and S^{2-} (eq 2.5).[29] In the presence of H^+, $S_2O_3^{2-}$ ions transformed to HSO_3^{2-} ions and S (eq 2.6). Finally, the generation of ZnS on the surface of ZnO/CdS occurred (eqs 2.7 and 2.8).

$$ZnO/CdS + h\nu \rightarrow ZnO/CdS(e_{CB}^- + h_{VB}^+) \quad (2.1)$$

$$SO_3^{2-} + H_2O + 2h_{VB}^+ \rightarrow SO_4^{2-} + 2H^+ \quad (2.2)$$

$$2S^{2-} + 2h_{VB}^+ \rightarrow S_2^{2-} \quad (2.3)$$

$$SO_3^{2-} + S^{2-} + 2h_{VB}^+ \rightarrow S_2O_3^{2-} \quad (2.4)$$

$$S_2^{2-} + SO_3^{2-} \rightarrow S_2O_3^{2-} + S^{2-} \quad (2.5)$$

$$S_2O_3^{2-} + H^+ \rightarrow HSO_3^- + S \quad (2.6)$$

$$Zn^{2+} + S^{2-} \rightarrow ZnS \quad (2.7)$$

$$Zn^{2+} + S + 2e^- \rightarrow ZnS \quad (2.8)$$

To confirm the generation of ZnS, we investigated the structure of recycle ZnO/CdS-T120 photocatalyst (denoted as ZnO/CdS-T120-R). Figure 4a shows XRD patterns of ZnO/CdS-T120 and ZnO/CdS-T120-R. Compared with fresh ZnO/CdS-T120, a new diffraction peak at 28.7° appeared for the recycle sample, which was assigned to the (111) plane of wurtzite ZnS (JCPDS No. 05-0566). In addition, the peak intensity of ZnO decreased after the formation of ZnS on the surface. Figure 4b presents the TEM micrograph of ZnO/CdS-T120-R. It was clearly observed that lots of ZnS particles with size of several nanometers accumulated on the surface. Figure 4c gives the EDX spectrum of ZnO/CdS-T120-R. Elemental Zn, O, Cd, and S were found. Meanwhile, the stronger signal intensity for S element demonstrated that the amount of S was significantly increased for ZnO/CdS-T120-R, which was mostly due to the generation of ZnS. Figure 4d depicts a representative high-resolution TEM micrograph of ZnO/CdS-T120-R. The new lattice fringe with spacing 0.32 nm was in good agreement with the interplanar spacing of the (111) plane of ZnS, which was consistent with XRD analysis. Figure 4e presents the typical HRTEM images of CdS−ZnS interfaces, ZnO−ZnS interfaces, and CdS−ZnO−ZnS interfaces. The scanning TEM (STEM) image and the corresponding EDX elemental mapping images

DOI: 10.1021/acssuschemeng.5b00102
ACS Sustainable Chem. Eng. 2015, 3, 969−977

of Zn, Cd, O, and S are presented in Figure 4f. As shown, elemental Cd was nonuniformly dispersed on the ZnO surface, which was ascribed to the uncontrollable photodeposition preparation of CdS. However, elemental S was highly dispersed. This was because of the generation of ZnS on the ZnO surface that was not occupied by CdS in ZnO/CdS-T120-R.

To investigate the role of ZnS in photocatalytic H_2 evolution, we compared the H_2 evolution activities of ZnO/CdS-T120 and ZnO/CdS-T120-R using sulfur-free triethanolamine (10 vol %) as a hole scavenger. The results are presented in Figure 5a. The photocatalytic H_2 evolution rate of ZnO/CdS-T120-R was about 4.5 times higher than that of ZnO/CdS-T120. At the same time, to further explore the correlation between the ZnS content and catalytic activity, the H_2 evolution rates for those with different ZnS contents were discussed in the photocatalytic system using sulfur-free triethanolamine (10 vol %) as a hole scavenger. According to our previous study, it was confirmed that the content of in situ generative ZnS increased with the increasing Na_2S concentration used.[25] Therefore, we adopted such strategy to control the amount of ZnS generation. Figure 5b presents the difference values of photocatalytic H_2 evolution rate versus the difference values of generative ZnS. As the weight percents of ZnS increased by 4.00, 8.73, and 17.10% (determined by ICP-AES), respectively, the corresponding H_2 evolution rates increased by 65, 101, and 143 μmol g^{-1} h^{-1}. Evidently, an increase of ZnS content contributed to the enhancement of H_2 evolution activity. These results strongly indicated that the formation of ZnS on ZnO/CdS surface could enhance photocatalytic H_2 evolution activity for ZnO/CdS. Subsequently, the optical adsorption properties of ZnO/CdS-T120 and ZnO/CdS-T120-R were compared, as shown in Figure 5c. ZnO/CdS-T120 had a visible light absorption band from 400 to ca. 560 nm due to the strong absorption of CdS in the visible light region. However, in comparison with ZnO/CdS-T120, ZnO/CdS-T120-R showed a slight red shift and a more wide visible light absorption band from 400 to ca. 610 nm was observed. These results can be explained by the presence of ZnS, which extended the visible light adsorption region of ZnO/CdS.[26]

HRTEM images of ZnO/CdS-T120 (Figure 1d) and ZnO/CdS-T120-R (Figure 4d,e) clearly reveal the intimate contact among ZnS, ZnO, and CdS particles. Therefore, besides the transfer of photogenerated electrons and holes that occurred in the ZnO−CdS interface, ZnO−ZnS, CdS−ZnS and CdS−ZnO−ZnS interfaces also possibly provided the effective photogenerated charge carriers transfer. Therefore, as presented in Scheme 1, in ZnO−CdS interfaces (pathway 1), because ZnO is visible light inactive and the conduction band edge potential of CdS is more negative than that of ZnO, a difference in band potentials between them formed.[30−33] Then the photogenerated electrons were driven from CdS to ZnO under visible light irradiation by the electric field created at their interfaces for water reduction, while the generated holes remained in CdS would be subjected to quenching by the sacrificial agents. In ZnS−CdS interfaces (pathway 2), ZnS has both a higher conduction band and a deeper valence band,[34,35] CdS can be effectively photogenerated under visible light irradiation, and ZnS is visible light inactive. The photogenerated electrons were used for water reduction. The holes could be transferred from CdS to the localized acceptor states above the valence band of ZnS though the conduct band and valence band of ZnS were higher and lower than those of CdS, respectively. The localized acceptor states were caused by zinc

Scheme 1. Graphical Representation for the Photocatalytic H_2 Production Mechanism

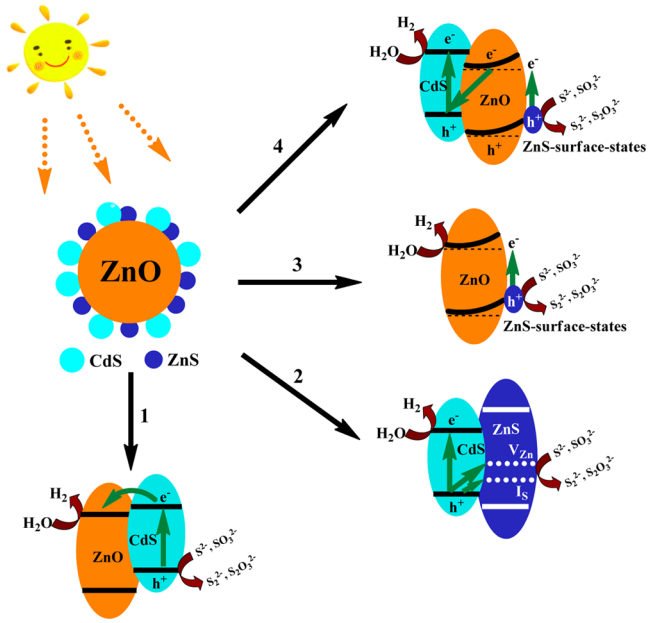

vacancies (V_{Zn}) and interstitial sulful (I_S) existed in ZnS crystal,[36] which had been confirmed based on the luminescence study on ZnO/CdS-T120-R in this work (see the Supporting Information, Figure S5). The acceptor states of V_{Zn} were higher than those of the I_S atoms.[37] In ZnO−ZnS interfaces (pathway 3), the electrons at the ZnO−ZnS interfaces could be excited under visible light irradiation from the bent valence band level to the conduction bend of ZnO for water reduction while the photogenerated holes trapped by ZnS-surface-states were subjected to quenching by the sacrificial reagent, which have been reported in our previous study.[25] In CdS−ZnO−ZnS interfaces (pathway 4), a Z-scheme mechanism was developed that was consistent with previously reported studies.[21,23] Under visible light irradiation, ZnO (the presence of ZnS-surface-states) and CdS were photogenerated. The conduct band electrons from ZnO combined with the valence band holes of CdS. The remaining conduct band electrons in CdS were for further reaction to generate H_2 gas. Meanwhile, the valence band holes in ZnO trapped by ZnS-surface-states were subjected to quenching by the sacrificial reagent. Obviously, it was concluded that the formation of ZnS increased the transfer interfaces for photogenerated charge carriers and consequently promoted the separation of photogenerated electrons and holes.

CONCLUSIONS

In conclusion, a novel preparation strategy for ZnO/CdS hybrid photocatalysts was designed and realized by a simple and reducible photodeposition method. The content of CdS loading can be adjusted by the change of irradiation time. ZnO/CdS-T120 showed the highest H_2 evolution rate (1725 μmol g^{-1} h^{-1}), which was about 9.2 and 34.5 times than that of compared ZnO and CdS photocatalysts. Additionally, ZnO/CdS-T120 presented stable photocatalytic H_2 evolution activity and good natural sunlight driven H_2 evolution ability. Compared with other H_2 evolution photocatalysts, ZnO/CdS-T120 showed higher H_2 evolution activity and stability. ZnS formed on ZnO/CdS-T120 surface in the photocatalytic

DOI: 10.1021/acssuschemeng.5b00102
ACS Sustainable Chem. Eng. 2015, 3, 969−977

process, which enhanced the photocatalytic H_2 activity of ZnO/CdS and extended the visible light adsorption region. Meanwhile, the generation of ZnS increased the transfer interfaces for photogenerated charge carriers and consequently promoted the separation of photogenerated electrons and holes. This work may be significant to provide an insight into investigating the high photocatalytic H_2 activities for ZnO/CdS hybrid photocatalysts deeply and preparing CdS based composite photocatalytic materials with high activities for application in solar energy utilization and conversation.

■ ASSOCIATED CONTENT

Supporting Information

Table S1, contents of Cd element for different photocatalyst measured by ICP-AES; Table S2, comparison of visible light driven H_2 evolution activity for different photocatalysts; Figure S1, XRD patterns of pure ZnO and ZnO/CdS nanocomposites with different CdS loading; Figure S2, TEM images of ZnO/CdS-T30, ZnO/CdS-T60 and ZnO/CdS-T120; Figure S3, UV−vis diffuse reflectance spectra of ZnO/CdS under different irradiation times; Figure S4, photo of outdoor equipment of sunlight-driven water splitting by ZnO/CdS-T120 system in Wuxi city on July 22, 2014; Figure S5, luminescence spectrum fitted by four Gaussian curves in the range from 460 to 400 nm for ZnO/CdS-T120-R at the excitation wavelength of 285 nm. This material is available free of charge via the Internet at http://pubs.acs.org/.

■ AUTHOR INFORMATION

Corresponding Authors

*Y. Dong. Fax: +86 510 85917763. E-mail: dongym@jiangnan.edu.cn.

*P. Jiang. Fax: +86 510 85917763. E-mail: ppjiang@jiangnan.edu.cn.

Notes

The authors declare no competing financial interest.

■ ACKNOWLEDGMENTS

The authors gratefully acknowledge the support from the National Natural Science Foundation of China (No. 20903048 and No. 21275065), the Fundamental Research Funds for the Central Universities (JUSRP51314B, JUSRP13015), the Postgraduate Innovation Project of Jiangsu Province (CXZZ13-0743), and MOE & SAFEA for the 111 Project (B13025).

■ REFERENCES

(1) Chen, X.; Shen, S.; Guo, L.; Mao, S. S. Semiconductor-based photocatalytic hydrogen generation. *Chem. Rev.* **2010**, *110*, 6503−6570.

(2) Xiang, Q.; Yu, J.; Jaroniec, M. Synergetic effect of MoS_2 and graphene as cocatalysts for enhanced photocatalytic H_2 production activity of TiO_2 nanoparticles. *J. Am. Chem. Soc.* **2012**, *134*, 6575−6578.

(3) Martin, D. J.; Qiu, K.; Shevlin, S. A.; Handoko, A. D.; Chen, X.; Guo, Z.; Tang, J. Highly efficient photocatalytic H_2 evolution from water using visible light and structure-controlled graphitic carbon nitride. *Angew. Chem., Int. Ed.* **2014**, *53*, 9240−9245.

(4) Li, Z.-J.; Li, X.-B.; Wang, J.-J.; Yu, S.; Li, C.-B.; Tung, C.-H.; Wu, L.-Z. A robust "artificial catalyst" in situ formed from CdTe QDs and inorganic cobalt salts for photocatalytic hydrogen evolution. *Energy Environ. Sci.* **2013**, *6*, 465−469.

(5) Zong, X.; Yan, H.; Wu, G.; Ma, G.; Wen, F.; Wang, L.; Li, C. Enhancement of photocatalytic H_2 evolution on CdS by loading MoS_2 as cocatalyst under visible light irradiation. *J. Am. Chem. Soc.* **2008**, *130*, 7176−7177.

(6) Li, Y.; Hu, Y.; Peng, S.; Lu, G.; Li, S. Synthesis of CdS nanorods by an ethylenediamine assisted hydrothermal method for photocatalytic hydrogen evolution. *J. Phys. Chem. C* **2009**, *113*, 9352−9358.

(7) Zhang, W.; Wang, Y.; Wang, Z.; Zhong, Z.; Xu, R. Highly efficient and noble metal-free NiS/CdS photocatalysts for H_2 evolution from lactic acid sacrificial solution under visible light. *Chem. Commun.* **2010**, *46*, 7631−7633.

(8) Wang, Y.; Wang, Y.; Xu, R. Photochemical deposition of Pt on CdS for H_2 evolution from water: Markedly enhanced activity by controlling Pt reduction environment. *J. Phys. Chem. C* **2013**, *117*, 783−790.

(9) Zhao, Q.; Ji, M.; Qian, H.; Dai, B.; Weng, L.; Gui, J.; Zhang, J.; Ouyang, M.; Zhu, H. Controlling structural symmetry of a hybrid nanostructure and its effect on efficient photocatalytic hydrogen evolution. *Adv. Mater.* **2014**, *26*, 1387−1392.

(10) Li, Z.-J.; Wang, J.-J.; Li, X.-B.; Fan, X.-B.; Meng, Q.-Y.; Feng, K.; Chen, B.; Tung, C.-H.; Wu, L.-Z. An exceptional artificial photocatalyst, Ni_h-CdSe/CdS core/shell hybrid, made in situ from CdSe quantum dots and nickel salts for efficient hydrogen evolution. *Adv. Mater.* **2013**, *25*, 6613−6618.

(11) Huang, L.; Wang, X.; Yang, J.; Liu, G.; Han, J.; Li, C. Dual cocatalysts loaded type I CdS/ZnS core/shell nanocrystals as effective and stable photocatalysts for H_2 evolution. *J. Phys. Chem. C* **2013**, *117*, 11584−11591.

(12) Challa, K. K.; Goswami, S. K.; Oh, E.; Kim, E. T. Effect of CdS film thickness on the photoexcited carrier lifetime of TiO_2/CdS core-shell nanowires. *Appl. Phys. Lett.* **2011**, *99*, 153111.

(13) Zhang, L. J.; Li, S.; Liu, B. K.; Wang, D. J.; Xie, T. F. Highly efficient CdS/WO_3 photocatalysts: Z-Scheme photocatalytic mechanism for their enhanced photocatalytic H_2 evolution under visible light. *ACS Catal.* **2014**, *4*, 3724−3729.

(14) Daskalaki, V. M.; Antoniadou, M.; Puma, G. L.; Kondarides, D. I.; Lianos, P. Solar light-responsive Pt/CdS/TiO_2 photocatalysts for hydrogen production and simultaneous degradation of inorganic or organic sacrificial agents in wastewater. *Environ. Sci. Technol.* **2010**, *44*, 7200−7205.

(15) Antoniadou, M.; Daskalaki, V. M.; Balis, N.; Kondarides, D. I.; Kordulis, C.; Lianos, P. Photocatalysis and photoelectrocatalysis using (CdS-ZnS)/TiO_2 combined photocatalysts. *Appl. Catal., B* **2011**, *107*, 188−196.

(16) Kim, H.; Kim, J.; Kim, W.; Choi, W. Enhanced photocatalytic and photoelectrochemical activity in the ternary hybrid of CdS/TiO_2/WO_3 through the cascadal electron transfer. *J. Phys. Chem. C* **2011**, *115*, 9797−9805.

(17) Yang, G.; Yan, W.; Zhang, Q.; Shen, S.; Ding, S. One-dimensional CdS/ZnO core/shell nanofibers via single-spinneret electrospinning: Tunable morphology and efficient photocatalytic hydrogen production. *Nanoscale* **2013**, *5*, 12432−12439.

(18) Wang, X.; Liu, G.; Lu, G. Q.; Cheng, H.-M. Stable photocatalytic hydrogen evolution from water over ZnO-CdS core-shell nanorods. *Int. J. Hydrogen Energy* **2010**, *35*, 8199−8205.

(19) Wang, X.; Yin, L.; Liu, G.; Wang, L.; Saito, R.; Lu, G. Q.; Cheng, H.-M. Polar interface-induced improvement in high photocatalytic hydrogen evolution over ZnO-CdS heterostructures. *Energy Environ. Sci.* **2011**, *4*, 3976−3979.

(20) Vaishnav, J. K.; Arbuj, S. S.; Rane, S. B.; Amalnerkar, D. P. One dimensional CdS/ZnO nanocomposites: An efficient photocatalyst for hydrogen generation. *RSC Adv.* **2014**, *4*, 47637−47642.

(21) Wang, X.; Liu, G.; Chen, Z.-G.; Li, F.; Wang, L.; Lu, G. Q.; Cheng, H.-M. Enhanced photocatalytic hydrogen evolution by prolonging the lifetime of carriers in ZnO/CdS heterostructures. *Chem. Commun.* **2009**, 3452−3454.

(22) Zou, X.; Wang, P.-P.; Li, C.; Zhao, J.; Wang, D.; Asefa, T.; Li, G.-D. One-pot cation exchange synthesis of 1D porous CdS/ZnO heterostructures for visible-light-driven H_2 evolution. *J. Mater. Chem. A* **2014**, *2*, 4682−4689.

DOI: 10.1021/acssuschemeng.5b00102
ACS Sustainable Chem. Eng. 2015, 3, 969−977

(23) Peng, F.; Zhou, Q.; Zhang, D.; Lu, C.; Ni, Y.; Kou, J.; Wang, J.; Xu, Z. Bio-inspired design: Inner-motile multifunctional ZnO/CdS heterostructures magnetically actuated artificial cilia film for photocatalytic hydrogen evolution. *Appl. Catal., B* **2015**, *165*, 419−427.
(24) Arai, T.; Senda, S.; Sato, Y.; Takahashi, H.; Shinoda, K.; Jeyadevan, B.; Tohji, K. Cu-Doped ZnS hollow particle with high activity for hydrogen generation from alkaline sulfide solution under visible light. *Chem. Mater.* **2008**, *20*, 1997−2000.
(25) Zhao, H.; Dong, Y.; Jiang, P.; Wu, X.; Wu, R.; Chen, Y. Facile preparation of a ZnS/ZnO nanocomposite for robust sunlight photocatalytic H_2 evolution from water. *RSC Adv.* **2015**, *5*, 6494−6500.
(26) Wu, L. P.; Zhang, Y. L.; Long, L. Z.; Cen, C. P.; Li, X. J. Effect of ZnS buffer layers in ZnO/ZnS/CdS nanorod array photoelectrode on the photoelectrochemical performance. *RSC Adv.* **2014**, *4*, 20716−20721.
(27) Fujii, M.; Nagasuna, K.; Fujishima, M.; Akita, T.; Tada, H. Photodeposition of CdS quantum dots on TiO_2: Preparation, characterization, and reaction mechanism. *J. Phys. Chem. C* **2009**, *113*, 16711−16716.
(28) Gomathisankar, P.; Hachisuka, K.; Katsumata, H.; Suzuki, T.; Funasaka, K.; Kaneco, S. Photocatalytic hydrogen production from aqueous Na_2S + Na_2SO_3 solution with B-doped ZnO. *ACS Sustainable Chem. Eng.* **2013**, *1*, 982−988.
(29) Bao, N.; Shen, L.; Takata, T.; Domen, K. Self-templated synthesis of nanoporous CdS nanostructures for highly efficient photocatalytic hydrogen production under visible light. *Chem. Mater.* **2008**, *20*, 110−117.
(30) Rakshit, T.; Mondal, S. P.; Manna, I.; Ray, S. K. CdS-Decorated ZnO nanorod heterostructures for improved hybrid photovoltaic devices. *ACS Appl. Mater. Interfaces* **2012**, *4*, 6085−6095.
(31) Zhai, J.; Wang, L.; Wang, D.; Li, H.; Zhang, Y.; He, D.; Xie, T. Enhancement of gas sensing properties of CdS nanowire/ZnO nanosphere composite materials at room temperature by visible-light activation. *ACS Appl. Mater. Interfaces* **2011**, *3*, 2253−2258.
(32) Khanchandani, S.; Kundu, S.; Patra, A.; Ganguli, A. K. Shell thickness dependent photocatalytic properties of ZnO/CdS core-shell nanorods. *J. Phys. Chem. C* **2012**, *116*, 23653−23662.
(33) Shen, Q.; Zhao, X.; Zhou, S.; Hou, W.; Zhu, J.-J. ZnO/CdS Hierarchical nanospheres for photoelectrochemical sensing of Cu^{2+}. *J. Phys. Chem. C* **2011**, *115*, 17958−17964.
(34) Xie, Y. P.; Yu, Z. B.; Liu, G.; Ma, X. L.; Cheng, H.-M. CdS-Mesoporous ZnS core-shell particles for efficient and stable photocatalytic hydrogen evolution under visible light. *Energy Environ. Sci.* **2014**, *7*, 1895−1901.
(35) Zhang, J.; Wang, L.; Liu, X.; Li, X.; Huang, W. High-performance CdS-ZnS core-shell nanorod array photoelectrode for photoelectrochemical hydrogen generation. *J. Mater. Chem. A* **2015**, *3*, 535−541.
(36) Becker, W. G.; Bard, A. J. Photoluminescence and photoinduced oxygen adsorption of colloidal zinc sulfide dispersions. *J. Phys. Chem.* **1983**, *87*, 4888−4893.
(37) Denzler, D.; Olschewski, M.; Sattler, K. Luminescence studies of localized gap states in colloidal ZnS nanocrystals. *J. Appl. Phys.* **1998**, *84*, 2841−2845.

DOI: 10.1021/acssuschemeng.5b00102
ACS Sustainable Chem. Eng. 2015, 3, 969−977